Multi-Waveform STAP

Shannon D. Blunt[1], John Jakabosky[1], Justin Metcalf[1], James Stiles[1], and Braham Himed[2]
[1] Radar Systems Lab, University of Kansas, Lawrence, KS
[2] Sensors Directorate, Air Force Research Lab, Dayton, OH

***Abstract* – A new form of Space-Time Adaptive Processing (STAP) is introduced that is amenable to the simultaneous transmission of multiple-input multiple-output (MIMO) emissions from an airborne/space-based platform. Denoted as Multi-Waveform STAP (MuW-STAP or simply μ-STAP), this receive scheme incorporates new sources of training data for the STAP sample covariance matrix through the use of "orthogonal" waveforms optimized for use on a physical system. This additional training data improves robustness to both heterogeneous clutter and target contamination of training data, and also reduces the false alarms that would otherwise occur due to residual clutter.**

I. INTRODUCTION

For airborne/space-based radar performing ground moving target indication (GMTI) the motion of the platform necessitates the use of a coupled space-time receive filter to cancel clutter effectively. In general, space-time adaptive processing (STAP) schemes realize this receive filter by estimating the covariance matrix of the clutter that resides in a given cell-under-test (CUT) and within which a target may likewise exist [1]. Estimation of this covariance matrix necessitates the existence of training data whose space-time characteristics are homogenous with that in the CUT. However, due to the tendency for clutter to be non-stationary in range and azimuth, internal clutter motion, the possible contamination of training data by targets of interest, and limited sample support, accurate estimation of the clutter covariance matrix remains one of the most difficult aspects of a practical STAP implementation [2,3].

The multiple-input multiple-output (MIMO) paradigm, originally developed for communication applications, has been suggested for use in sensing modalities. While numerous theoretical studies exist [4], the practical implementation of MIMO to radar has thus far been primarily limited to over-the-horizon (OTH) applications [5,6] and as a means to synchronize spatially distributed transmitters [7]. For GMTI, the oft-proposed MIMO trade-off between spatial directivity and dwell time may not be feasible due to short decoherence time and "range walking" effects for moving targets [8]. As such, the benefit of a traditional focused mainbeam must be balanced against the possible diversity afforded by the spatially-diffused emissions of multiple waveforms. Furthermore, these waveforms must be physically realizable and thus must be continuous, relatively bandlimited signals that are amenable to a physical transmitter [8,9]. Finally, given the feasible (non-zero) cross-correlation that can be achieved for a set of waveforms with respect to the high dynamic range for the receive powers of clutter, targets, and noise, the assumption of waveform "orthogonality" is not appropriate, though this loose vernacular will still be used here to be succinct.

These requirements as well as other physical constraints lead to a set of practical attributes summarized in Table 1. Given a finite power source, the loss of power to a focused mainbeam due to concurrent MIMO emissions involves a trade-off between energy on target (i.e. detection probability) and any diversity-induced enhancement to clutter suppression. Likewise, power efficiency necessitates operation of power amplifiers in saturation, which requires constant modulus, relatively bandlimited waveforms to minimize transmitter distortion. That said, only the mainbeam requires high power; thus amplitude modulation could be feasible for lower power signal components. In designing simultaneous emissions from different antenna elements that produce coupling in the space and fast-time dimensions one must also consider the fidelity limitation imposed by imperfect array calibration and mutual coupling between elements [10].

Table 1. Practical aspects for MIMO GMTI

1) Minimize loss of mainbeam power
2) Physical emissions (continuous, bandlimited waveforms)
3) Constant modulus waveforms for high power mainbeam
4) Non-zero waveform cross-correlation (not orthogonal)
5) Non-ideal antenna array (calibration, mutual coupling)

With this litany of practical constraints in mind, we propose a pragmatic approach to incorporating MIMO into the airborne/space-based GMTI modality as a means to enhance the segregation of sidelobe clutter and thereby enhance target detection and reduce false alarms. In so doing, a new receive filtering scheme denoted as Multi-Waveform STAP (MuW-STAP, or just μ-STAP) is introduced that leverages the resulting new source of space-time training data to improve clutter cancellation. In fact, it is observed that "orthogonal" pulse compression filters can realize much of this benefit even without the emission of additional waveforms.

II. PHYSICAL MIMO EMISSIONS

Because the term MIMO refers to several different instantiations, let us restrict our attention to space / fast-time

This work was supported in part by a subcontract with Booz, Allen and Hamilton for research sponsored by the Air Force Research Laboratory (AFRL) under Contract FA8650-11-D-1011.

coupling (SFTC) on transmit. This diversity scheme includes traditional beamforming at one extreme and at the other the notion of a different waveform simultaneously emitted from each individual antenna element. In light of the practical constraints discussed above, consider the following MIMO emission design.

A. Spatial Aspects

Let us denote a *primary* emission in the spatial look direction θ_{prime} with respect to antenna boresight along with $k = 1, \cdots, K$ *secondary* emissions. The primary emission comprises the mainbeam that is steered in the desired look direction to search for moving targets and is essentially the standard beamformed emission for GMTI. In contrast, the secondary emissions are used only to illuminate the clutter in spatial sidelobe directions so as to better affect its cancellation on receive. For example, Fig. 1 illustrates the case of $K = 1$ in which the primary emission is directed towards boresight and the single lower power secondary emission realizes a spatial null in the boresight direction. In this way the primary and secondary emissions are spatial orthogonal (or at least approximately so) in the direction of interest. While the secondary spatial null is certainly beneficial, it has actually been found that the proposed receiver scheme detailed in Section III provides a performance benefit as long as the secondary emission does not experience sufficient gain in the desired look direction.

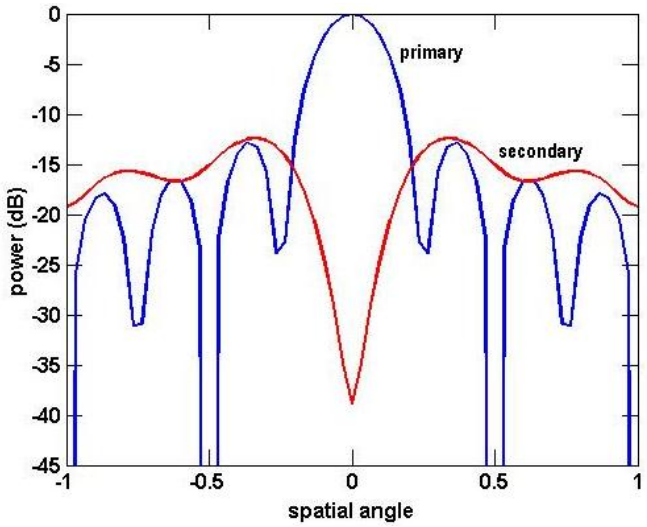

Figure 1. MIMO spatial beampattern

The relative powers of the primary and secondary emissions remains a topic of ongoing investigation. Clearly, the combined power cannot exceed the total amount provided by the power supply. Also note that, since the goal is to aggregate the clutter response into a covariance matrix, it is not necessary to obtain a "focused" clutter response; hence the low power, spatially diffused secondary beam. It is presumed that the secondary emissions can be produced by some secondary antenna structure or through a parsimonious allocation of elements into a small secondary sub-array.

B. Fast-time (Waveform) Aspects

With regard to the attributes of the set of $K+1$ total waveforms, it is only necessary for the waveform $s_{\text{prime}}(t)$ associated with the primary emission to possess the traditional characteristics of low range sidelobes (and perhaps Doppler tolerance). As such the primary waveform is essentially the same as one would use for traditional GMTI. In contrast, the secondary waveforms $s_{\text{sec},k}(t)$ for $k = 1, \cdots, K$ do not require low range sidelobes as it is not their purpose to focus the clutter. However, to optimize performance it is necessary to design the waveforms such that

$$\min_{s_{\text{prime}}(t),\, s_{\text{sec},k}(t)} \iint s_{\text{prime}}(t)\; s^{*}_{\text{sec},k}(t-\tau)\; dt\, d\tau \quad \forall k\,. \qquad (1)$$

In other words, the secondary waveforms need only have a low cross-correlation with the primary waveform. The optimization of continuous waveforms in this manner can be performed by using the continuous phase modulation (CPM) implementation described in [9]. For example, Fig. 2 depicts the autocorrelation and cross-correlation of two optimized CPM-implemented waveforms having a time-bandwidth product of ≈ 65 (nonlinear FM (NLFM) waveforms generated from length 65 codes). These waveforms are continuous and relatively bandlimited (spectral spreading is dominated by the rise/fall-time of the pulse).

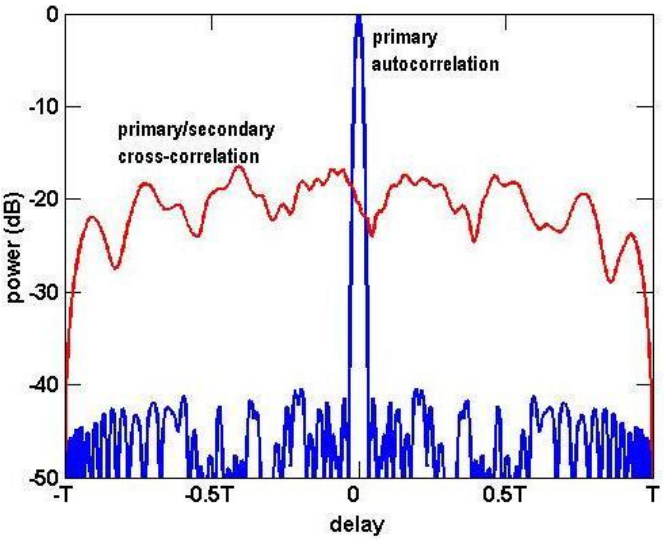

Figure 2. Auto/cross-correlations of two optimized NLFM waveforms

C. The SFTC Emission and Response

The purpose of the primary emission is identical to the standard GMTI illumination that has a high gain in the spatial look direction and for which the resulting echoes are focused in range via standard pulse compression. Given M pulses in the coherent processing interval (CPI) and N receive antenna elements, the data collected through the MN space-time receive channels are used to implement STAP.

The secondary emissions, being focused in neither space nor range, yield a defocused response that produces an aggregation of the clutter. This lack of focusing provides the

means with which to obtain a new source of training data for covariance matrix estimation that does not require exclusion of guard cells or the cell-under-test (CUT), which is normally necessary to avoid target self-cancellation.

III. MULTI-WAVEFORM STAP

The received signal for the m^{th} pulse in a CPI that is incident upon the n^{th} antenna element is the superposition of the reflections from primary and secondary emissions as

$$y(m,n,t) = s_{\text{prime}}(t) * x_{\text{prime}}(t) + \sum_{k=1}^{K} s_{\text{sec},k}(t) * x_{\text{sec},k}(t) + v(t) \quad (2)$$

where $x_{\text{prime}}(t)$ comprises the echoes from the primary waveform, $x_{\text{sec},k}(t)$ are the echoes from the k^{th} secondary waveform, the operation $*$ represents convolution, and $v(t)$ is additive noise. Receiver pulse compression according to each of the K+1 transmitted waveforms produces the set of signals defined as

$$\begin{aligned} z_{\text{prime}}(m,n,t) &= h_{\text{prime}}(t) * y(m,n,t) \\ z_{\text{sec},1}(m,n,t) &= h_{\text{sec},1}(t) * y(m,n,t) \\ &\vdots \\ z_{\text{sec},K}(m,n,t) &= h_{\text{sec},K}(t) * y(m,n,t) \end{aligned} \quad (3)$$

where $h_{\text{prime}}(t)$ is the pulse compression filter corresponding to the primary waveform and $h_{\text{sec},k}(t)$ is the pulse compression filter corresponding to the k^{th} secondary waveform. The pulse compression filters may be matched filters or some form of mismatch filters.

For look direction θ_{prime} the spatial steering vector $\mathbf{c}_{\text{s}}(\theta_{\text{prime}})$ can be formed to maximize the gain on the N-element receive antenna array. Likewise a temporal steering vector $\mathbf{c}_{\text{t}}(\omega_{\text{Dop}})$ can be formed to maximize the gain over the set of M pulses for the Doppler frequency ω_{Dop} corresponding to radial motion with respect to the radar platform. Thus the space-time steering vector is, as usual, formed as

$$\mathbf{c}_{\text{st}}(\theta_{\text{prime}}, \omega_{\text{Dop}}) = \mathbf{c}_{\text{t}}(\omega_{\text{Dop}}) \otimes \mathbf{c}_{\text{s}}(\theta_{\text{prime}}) \quad (4)$$

where $\otimes$ is the Kronecker product. The pulse compressed outputs from (3) are organized in the same manner as the space-time steering vector thereby yielding sets of length-NM space-time snapshots denoted as $\mathbf{z}_{\text{prime}}(t)$ corresponding to the primary waveform and $\mathbf{z}_{\text{sec},k}(t)$ for $k = 1,\ldots, K$ corresponding to each of the K secondary waveforms. Sampling in fast-time t results in the range cell (delay) index ℓ.

For standard STAP, estimation of the covariance matrix $\mathbf{R}(\ell_{\text{CUT}})$ corresponding to the cell-under-test (CUT) involves the focused (primary) snapshots as

$$\mathbf{R}(\ell_{\text{CUT}}) = E\left[\mathbf{z}_{\text{prime}}(t)\, \mathbf{z}_{\text{prime}}^{H}(t)\right] \approx \frac{1}{n(L)} \sum_{\substack{\ell \in L \\ \ell \neq \ell_{\text{CUT}}}} \mathbf{z}_{\text{prime}}(\ell)\, \mathbf{z}_{\text{prime}}^{H}(\ell) \quad (5)$$

where $(\bullet)^{H}$ signifies complex conjugation, $E[\bullet]$ denotes expectation, $n(L)$ is the number of snapshots in the set L, and $\ell_{\text{CUT}} \notin L$ to avoid nulling a possible target. The right side of (5) indicates the use of training data snapshots (indexed by ℓ) surrounding the CUT in range, with guard cells and non-homogeneity detection to excise outliers as necessary (e.g. [3,11,12]), to approximate the expectation via a sample covariance matrix (SCM). The standard STAP filter is formed as

$$\mathbf{w}(\ell_{\text{CUT}}, \theta_{\text{prime}}, \omega) = \mathbf{R}^{-1}(\ell_{\text{CUT}})\ \mathbf{c}_{\text{st}}(\theta_{\text{prime}}, \omega) \quad (6)$$

for application to the CUT snapshot as

$$\alpha(\ell_{\text{CUT}}) = \mathbf{w}^{H}(\ell_{\text{CUT}}, \theta_{\text{prime}}, \omega)\ \mathbf{z}_{\text{prime}}(\ell_{\text{CUT}}). \quad (7)$$

The resulting value $\alpha(\ell_{\text{CUT}})$ is then compared to a threshold (e.g. generated via CFAR detector) to ascertain the presence of a target.

For the new multi-waveform STAP formulation there are, in general, two ways in which the space-time snapshots generated by the secondary pulse compression filters in (3) may be used with regard to covariance matrix estimation. First, a new sample covariance matrix (SCM) can be defined by supplementing (5) as

$$\mathbf{R}_{\mu}(\ell_{\text{CUT}}) = E\left[\mathbf{z}_{\text{prime}}(t)\, \mathbf{z}_{\text{prime}}^{H}(t)\right] + \sum_{k=1}^{K} E\left[\mathbf{z}_{\text{sec},k}(t)\, \mathbf{z}_{\text{sec},k}^{H}(t)\right] \quad (8)$$

where the primary portion is performed in the same manner as in (5). Following the determination of $\mathbf{R}_{\mu}(\ell_{\text{CUT}})$ from (8), it can be substituted into (6) for subsequent application to the CUT snapshot as in (7).

Alternatively, one could use the secondary data by itself without the primary training data. For this approach the SCM is defined as

$$\mathbf{R}_{\mu,\text{NP}}(\ell_{\text{CUT}}) = \sum_{k=1}^{K} E\left[\mathbf{z}_{\text{sec},k}(t)\, \mathbf{z}_{\text{sec},k}^{H}(t)\right], \quad (9)$$

where the subscript 'NP' indicates no primary data is used.

It is interesting to note that the set of "orthogonal" pulse compression filters in (3) can be applied even when no secondary waveforms are emitted (i.e. not a

MIMO emission). The subsequent application of the μ-STAP formulation via (8) or (9) followed by (6) and (7) is found to still provide a marked performance gain over standard STAP. Given the use of either the standard or MIMO emission, combined with the three methods to estimate the SCM from (5), (8), or (9), there are therefore a total of six different transmit/receive combinations for this multi-waveform architecture. The following evaluates the efficacy of these various combinations.

IV. Simulation Results

Consider an airborne side-looking radar. The STAP receive array is comprised of $N = 8$ uniform linear receive elements and the CPI consists of $M = 8$ pulses. The MIMO emission consists of a primary waveform and a single secondary waveform ($K = 1$). The specific waveforms employed here are those shown in Fig. 2 that were generated from the CPM implementation of length 65 optimized polyphase codes via [9].

The simulated noise is complex white Gaussian. The clutter is generated by dividing the range ring in azimuth into 61 equal-sized clutter patches, with the scattering from each patch i.i.d. complex Gaussian. This spatial clutter distribution is weighted by the transmit beampattern and scaled such that, following coherent integration (pulse compression, beamforming, and Doppler processing) without clutter cancellation, the average clutter-to-noise ratio (CNR) is 50 dB. To represent heterogeneous clutter [3], the power of the patches is randomly modulated as a function of range based on a uniformly distributed draw on [−10, 10] dB, the patches are modulated across azimuth (independent for each range ring) according to a randomly parameterized sinusoidal model, and internal clutter motion is incorporated that is distributed on ±0.02 normalized Doppler for each clutter patch.

For clutter cancellation, the sample covariance matrix (SCM) is formed via either (5), (8), or (9) according to the processing approach. For the primary training data, the cell-under-test (CUT) and 8 guard cells on either side of the CUT are excluded from the SCM that otherwise includes 64 primary training data vectors beyond each set of guard cells (for a total of 128). The secondary training data comprises the secondary data vectors corresponding to the same 128 range cells as well as those training data vectors associated with the guard cells and the CUT.

The results for probability of detection (P_d) are dependent on the target SNR, which is defined here as the output value after the coherent integration stages without clutter cancellation. The target has a normalized Doppler of 0.25. A cell-averaging CFAR (CA-CFAR) detector is applied that uses 30 range cells (15 before and 15 after) with 1 guard cell on either side of the CUT. The CFAR detector is based on a presumption of Gaussian-distributed data with a quiescent P_{fa} of 10^{-4} thus resulting in a CFAR threshold of 10.78 dB [13].

Six different combinations of GMTI transmit/receive schemes are considered as outlined in Table 2. On transmit these combinations are comprised of either the standard emission (1 waveform) or the MIMO emission scheme from Section II (here 2 waveforms), and on receive they employ standard STAP, μ-STAP, or μ-STAP (NP) which uses no primary training data in the SCM. To ensure full rank, the SCM for all cases is supplemented by diagonally loading with the noise power after pulse compression.

Table 2. Combinations of GMTI Tx/Rx methods

STAP	Tx: standard emission (1 waveform) Rx: standard STAP via (5)
μ-STAP	Tx: standard emission (1 waveform) Rx: μ-STAP via (8)
μ-STAP (NP)	Tx: standard emission (1 waveform) Rx: μ-STAP, **no primary** data via (9)
MIMO STAP	Tx: MIMO emission (two waveforms) Rx: standard STAP via (5)
MIMO μ-STAP	Tx: MIMO emission (two waveforms) Rx: μ-STAP via (8)
MIMO μ-STAP (NP)	Tx: MIMO emission (two waveforms) Rx: μ-STAP, **no primary** data via (9)

We first consider performance for homogeneous clutter. In Figs. 3 and 4 it is observed that the best detection performance is obtained when the μ-STAP (NP) approach is applied for the MIMO emission, followed very closely by μ-STAP applied to the standard emission. In contrast, the MIMO emission employing standard STAP yields the worst performance requiring 3.7 dB higher target SNR for a detection probability of 0.5. For the same P_d the standard STAP paradigm is only 0.8 dB better than the worst case. The benefit of the secondary training data is clear as the four approaches that employ it all perform better than the two implementations of standard STAP. This fact is likewise demonstrated when considering the false alarm probability in Figure 4, where it is found that the four configurations employing secondary training data result in P_{fa} values between 3×10^{-4} and 4×10^{-4} while the two standard STAP configurations produce P_{fa} values of 9×10^{-4}.

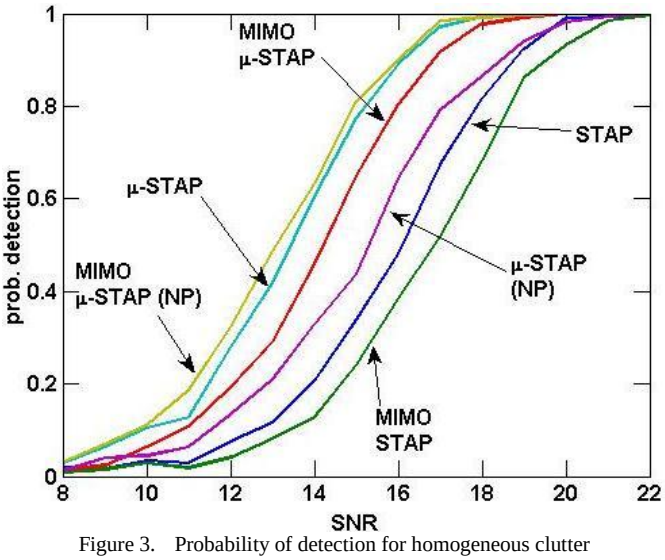

Figure 3. Probability of detection for homogeneous clutter

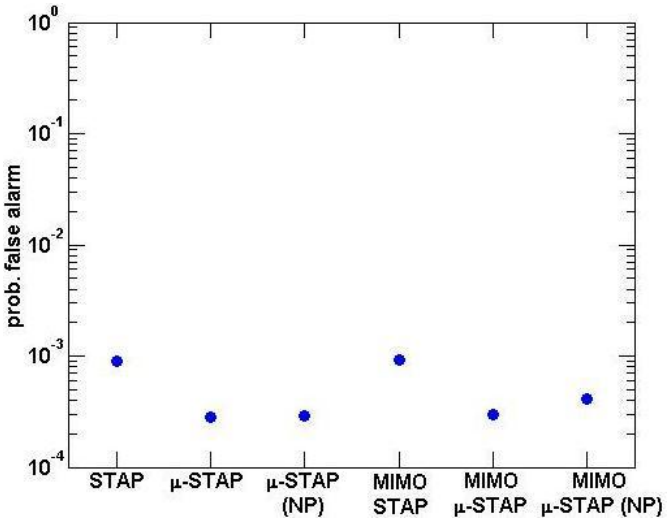

Figure 4. Probability of false alarm for homogeneous clutter

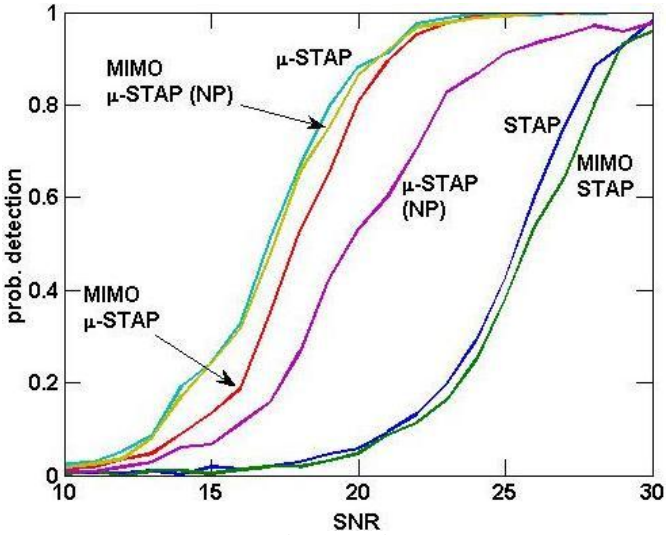

Figure 5. Probability of detection for heterogeneous clutter

Next we consider the effect of heterogeneous clutter. Figures 5 and 6 illustrate the detection and false alarm probability results for the six configurations. While all approaches fare worse for heterogeneous clutter, the two standard STAP approaches realize the most significant degradation. For a detection probability of 0.5, the best performers (μ-STAP for standard emission and MIMO μ-STAP (NP) are basically tied) and the worst performer (STAP for MIMO emission) now realize a difference of 8.9 dB. For the same P_d the standard STAP paradigm is now only 0.3 dB better than the worst case. In terms of false alarm probability the MIMO μ-STAP configuration is now the clear winner with an observed $P_{fa} = 4\times10^{-4}$, unchanged from the homogeneous clutter scenario. In contrast, the standard STAP approach experiences more than an order of magnitude increase in false alarm rate for heterogeneous clutter relative to homogeneous clutter. All other approaches have likewise experienced an increase in P_{fa} to varying degrees.

Finally, Figs. 7-10 illustrate anecdotal results from a single run of homogeneous clutter (40 dB CNR) in which four mainbeam targets (20 dB SNR) are present in nearby ranges with the same Doppler (the most distant targets are 40 range cells apart). Such a scenario is known to induce self-cancellation for standard STAP [2,3] and this effect is born out in Fig. 7 where only two of the targets exceed a common 10 dB CFAR threshold. In Fig. 8, μ-STAP (NP) applied to the standard emission detects three (and nearly all four) of the targets because it avoids use of the primary data that would cause self-cancellation. For the MIMO μ-STAP results in Fig. 9 the secondary data appears to temper some of the self-cancellation effect of the primary data, though not enough for more than two of the four targets to exceed the 10 dB threshold. Finally, Fig. 10 shows how MIMO μ-STAP (NP) is nominally able to detect all four targets due to the spatial and fast-time segregation between the secondary data and the focused primary data thereby minimizing self-cancellation effects.

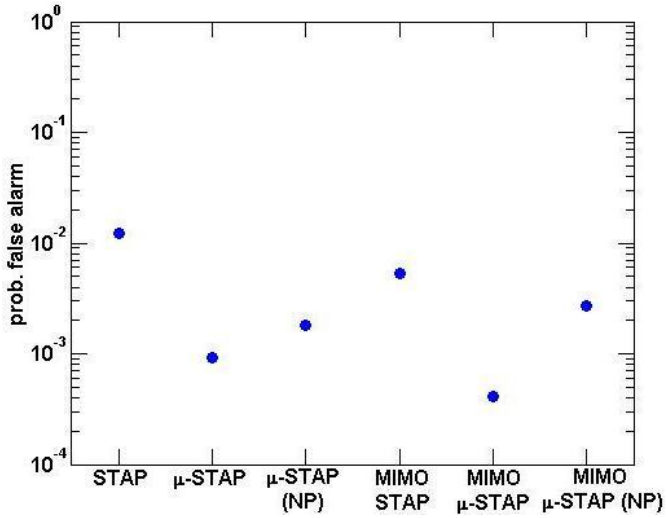

Figure 6. Probability of false alarm for heterogeneous clutter

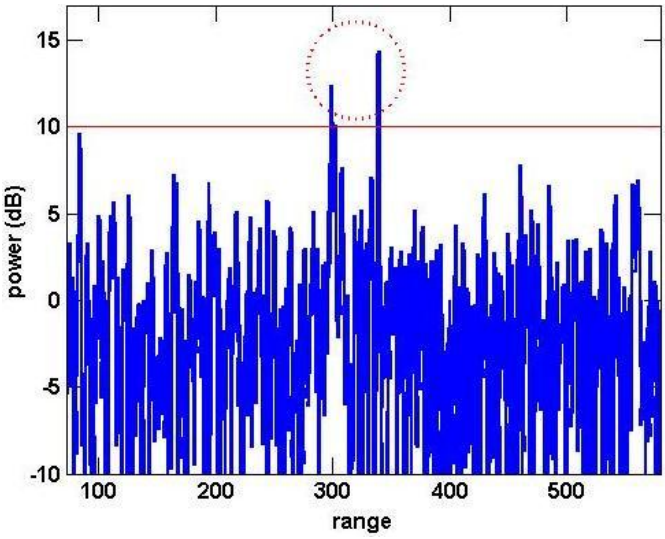

Figure 7. Standard emission, STAP, homogeneous clutter, 4 targets

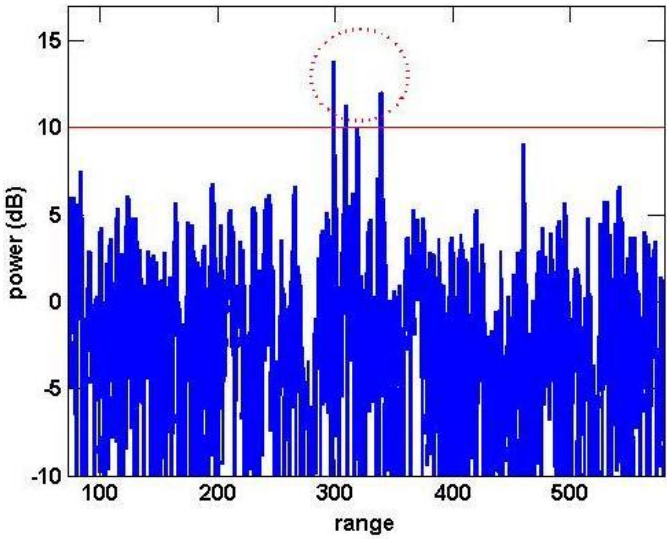

Figure 8. Standard emission, μ-STAP (NP), homogeneous clutter, 4 targets

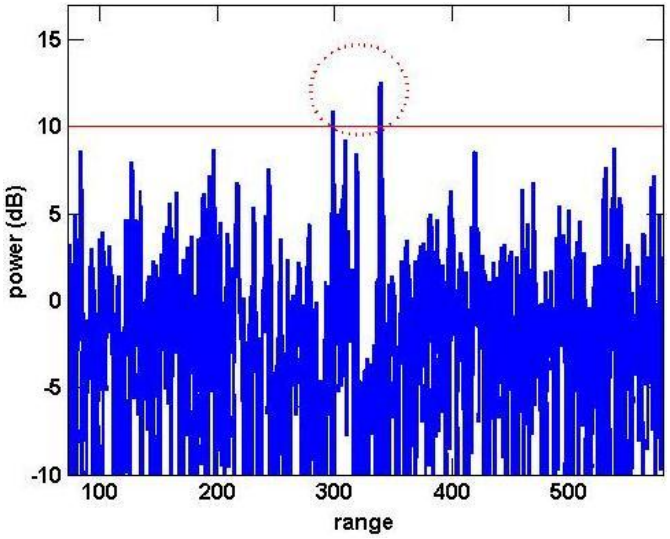

Figure 9. MIMO emission, μ-STAP, homogeneous clutter, 4 targets

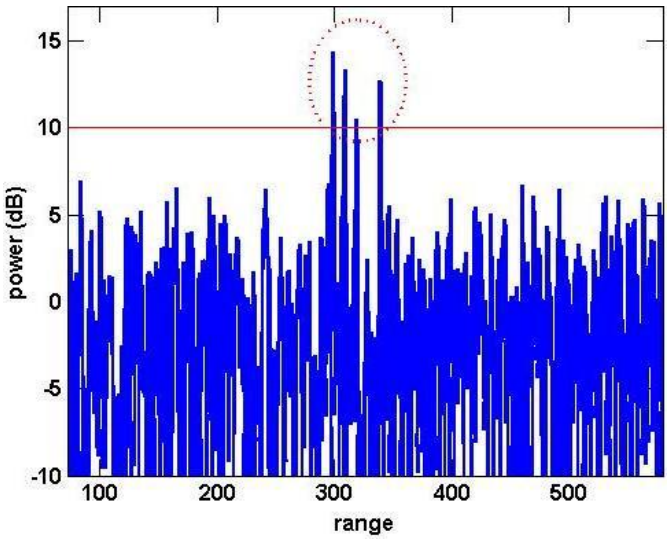

Figure 10. MIMO emission, μ-STAP (NP), homogeneous clutter, 4 targets

V. Conclusions

A multi-waveform approach to airborne GMTI has been presented that, on transmit, employs a minor deviation from standard beamforming to incorporate low-power secondary emissions. These secondary emissions illuminate spatial sidelobe clutter with waveforms that possess low cross-correlation with the primary waveform in the mainbeam. On receive a multi-waveform variant of STAP, denoted as μ-STAP, is used to incorporate the pulse compressed secondary data into the sample covariance matrix. Because this secondary data is unfocused and possesses low temporal correlation with the mainbeam echoes, it is possible to include the secondary data associated with the guard cells and the cell-under-test (CUT) in the sample covariance matrix with minimal impact to target self-cancellation. It was shown that the secondary training data provides needed robustness to heterogeneous clutter and target contamination of the primary training data. The secondary training data may also potentially provide the foundation for new forms of non-homogeneity detection and CFAR detection.

References

[1] J. Ward, "Space-time adaptive processing for airborne radar," *Lincoln Lab Tech. Report*, TR-1015, Dec. 1994.

[2] K. Gerlach, "Outlier resistance adaptive matched filtering," *IEEE Trans. AES*, pp. 885-901, July 2002.

[3] W.L. Melvin, "Space-time adaptive radar performance in heterogeneous clutter," *IEEE Trans. AES*, pp. 621-633, Apr. 2000.

[4] J. Li and P. Stoica, *MIMO Radar Signal Processing*, John Wiley & Sons, Inc., 2009.

[5] G.J. Frazer, Y.I. Abramovich, and B.A. Johnson, "Multiple-input multiple-output over-the-horizon radar: experimental results," *IET Radar, Sonar & Nav.*, pp. 290-303, 2009.

[6] R.J. Riddols, M. Ravan, and R.S. Adve, "Canadian HF over-the-horizon radar experiments using MIMO techniques to control auroral clutter," *IEEE Radar Conf.*, pp. 718-723, May 2010.

[7] S. Coutts, K. Cuomo, J. McHarg, F. Robey, and D. Weikle, "Distributed coherent aperture measurements for next generation BMD radar," *IEEE SAM Workshop*, pp. 390-393, July 2006.

[8] F.Daum and J. Huang, "MIMO radar: snake oil or good idea?," *IEEE AES Magazine*, pp. 8-12, May 2009.

[9] J. Jakabosky, S.D. Blunt, M.R. Cook, J. Stiles, and S.A. Seguin, "Transmitter-in-the-loop optimization of physical radar emissions," *IEEE Radar Conf.*, pp. 874-879, May 2012.

[10] B. Cordill, J. Metcalf, S.A. Seguin, D. Chatterjee, and S.D. Blunt, "The impact of mutual coupling on MIMO radar emissions," *IEEE Intl. Conf. on EM in Advanced Applications*, pp. 644-647, Sept. 2011.

[11] M. Rangaswamy, P. Chen, J.H. Michels, and B. Himed, "A comparison of two non-homogeneity detection methods for space-time adaptive processing," *IEEE SAM Workshop*, pp. 355-359, Aug. 2002.

[12] K. Gerlach, S.D. Blunt, and M.L. Picciolo, "Robust adaptive matched filtering using the FRACTA algorithm," *IEEE Trans. AES*, pp. 929-945, July 2004.

[13] M.A. Richards, J.A. Scheer, and W.A. Holm, *Principles of Modern Radar: Basic Principles*, SciTech, 2010, Sect. 16.5.